Available online at www.sciencedirect.com
SCIENCE DIRECT®
Journal of volcanology and geothermal research
ELSEVIER
Journal of Volcanology and Geothermal Research 150 (2006) 359–377
www.elsevier.com/locate/jvolgeores

Volcanic particle aggregation in explosive eruption columns. Part I: Parameterization of the microphysics of hydrometeors and ash

C. Textor [a,*], H.F. Graf [a,1], M. Herzog [a,2], J.M. Oberhuber [b,3], William I. Rose [c], G.G.J. Ernst [c,d,4]

[a] *Max-Planck-Institut für Meteorologie, Hamburg, Germany*
[b] *Deutsches Klimarechenzentrum GmbH, Hamburg, Germany*
[c] *Department of Geological Engineering and Sciences, Michigan Technological University, Houghton, MI, USA*
[d] *Department of Earth Sciences, University of Bristol, UK*

Received 16 September 2004; received in revised form 6 September 2005; accepted 16 September 2005
Available online 15 December 2005

Abstract

The aggregation of volcanic ash particles within the eruption column of explosive eruptions has been observed at many volcanoes. It influences the residence time of ash in the atmosphere and the radiative properties of the umbrella cloud. However, the information on the processes leading to aggregate formation are still either lacking or very incomplete. We examine the fate of ash particles through numerical experiments with the plume model ATHAM (Active Tracer High resolution Atmospheric Model) in order to determine the conditions that promote ash particle aggregation. In this paper we describe the microphysics and parameterization of ash and hydrometeors. In a companion paper (this issue) we use this information in a series of numerical experiments.

The parameterization includes the condensation of water vapor in the rising eruption column. The formation of liquid and solid hydrometeors and the effect of latent heat release on the eruption column dynamics are considered. The interactions of hydrometeors and volcanic ash within the eruption column that lead to aggregate formation are simulated for the first time within a rising eruption column. The microphysical parameterization follows a modal approach. The hydrometeors are described by two size classes, each of which is divided into a liquid and a frozen category. By analogy with the hydrometeor classification, we specify four categories of volcanic ash particles. We imply that volcanic particles are active as condensation nuclei for water and ice formation. Ash can be contained in all categories of hydrometeors, thus forming mixed particles of any composition reaching from mud rain to accretionary lapilli. Collisions are caused by gravitational capture of particles with different fall velocity. Coalescence of hydrometeor–ash aggregates is assumed to be a function of the hydrometeor mass fraction within the mixed particles. The parameterization also includes simplified descriptions of electrostatics and salinity effects.

Keywords: ash particle aggregation; cloud microphysics; numerical simulation; volcanic eruption column; hydrometeors; gas particle separation

* Corresponding author. Present address: Laboratoire des Sciences du Climat et de l'Environnement, Gif-sur-Yvette, France.
E-mail address: christiane.textor@gmx.de (C. Textor).
[1] Present address: Department of Geography, University of Cambridge, UK.
[2] Present address: NOAA Geophysical Fluid Dynamics Laboratory (GFDL), Princeton, USA.
[3] Now at a private company.
[4] Present adress: Mercator&Ortelius Research Centre for Eruption Dynamics, Department of Geology and Soil Science, University of Ghent, Belgium.

0377-0273/$ - see front matter © 2005 Elsevier B.V. All rights reserved.
doi:10.1016/j.jvolgeores.2005.09.007

1. Introduction

Strongly explosive volcanic eruptions with high-altitude eruption columns penetrating into the stratosphere have important effects on the environment, both on the local and on the global climate scale (e.g., Robock, 2000; Textor et al., 2004). The impact of volcanic ejecta depends on the strength of the eruption, and on the dispersal and residence time of gases and particles in the atmosphere. The observation of the processes within volcanic eruption columns from an explosive event is problematic due to their opacity and inhomogeneity. In this paper we focus on the fate of ash particles. The particles undergo a variety of modification processes in the eruption column, some of which are not even qualitatively understood. Particle qualities inferred from ash deposits do not necessarily reflect those during transport in the atmosphere. In addition, volcanic fallout occurs in large areas which cannot be completely covered by observation at the present time. Weather satellites and radar systems have been used to track drifting volcanic clouds (e.g., Wen and Rose, 1994; Rose et al., 2000, 2001, 2003; Lacasse et al., 2004). However, important characteristics of the particles in the eruption column have not been measured in situ. For example, the in-cloud shape and size of single particles and the particle size distribution typically have to be pre-supposed in order to retrieve total mass estimates from remote sensing (e.g., Schneider et al., 1999; Krotkov et al., 1999). Ash aggregation is not considered in the algorithms for volcanic ash retrievals by satellites (Wen and Rose, 1994; Guo et al., 2004b).

Numerical experiments are helpful to explore processes occurring in the eruption column. There are several numerical models available at the moment (for an overview see Textor et al., in press). A detailed description of the dynamics is achieved in the multi-phase models of Wohletz et al. (1984), Valentine and Wohletz (1989), Dobran and Neri (1993) and Neri and Macedonio (1996), Neri et al. (2002), Clarke et al. (2002). Their concept helps gain insight into the early dynamical development of an eruption column. However, it is much too expensive in terms of computer time and memory to consider a higher number of grid points and components, or microphysical processes in the eruption column. The models of Wilson (1976) and Woods (1988, 1993), Glaze et al. (1997), or Veitch and Woods (2000, 2002) on the other hand allow for consideration of a higher number of transported quantities. However, the representation of the dynamics in these models is much simpler than in the above-mentioned ones. Cloud microphysics is limited to the condensation process. Veitch and Woods (2001) account for particle aggregation within this concept using the Woods-model. See however the comment and reply of Textor and Ernst (2004) and Veitch and Woods (2004), respectively. The dispersion and sedimentation of tephra both in the proximal and distal regions of the volcano have been modeled using sedimentation models (e.g., Sparks et al., 1991, 1992; Bursik et al., 1992; Ernst et al., 1996; Bonadonna et al., 1998; Koyaguchi and Ohno, 2001; Bonadonna et al., 2002b; Riedel et al., 2003; Bonadonna and Phillips, 2003), for overviews see Sparks et al. (1997) and Bursik (1998). In the case of eruption column models of this type, simple relationships are used to calculate the variation of the eruption column width and vertical velocity with height, and particles settle at their individual terminal fall velocity from the margins of turbulent jets, plumes and intrusive gravity currents. These simple models, although they provide invaluable insights about fundamental processes, do not explicitly predict the dynamics, and microphysical processes are not considered. The fallout of ash at greater distances from the vent has also been numerically simulated assuming that dispersal is dominated by atmospheric motion described by the advection–diffusion equation rather than by the motion of the eruption column itself (e.g., Armienti et al., 1988; Barberi et al., 1990; Glaze and Self, 1990), but this approach is not physically sound for highly explosive, so-called Plinian eruptions (e.g., Bursik et al., 1992; Ernst et al., 1994; Bonadonna et al., 2002b; Bonadonna and Phillips, 2003). Armienti et al. (1988) have considered an additional term for particle aggregation.

In this study we use the ATHAM model (Oberhuber et al., 1998; Graf et al., 1999; Herzog et al., 2003) to investigate, in both time and space, processes leading to particle aggregation in the eruption column. This model explicitly simulates the dynamics (including turbulence) and thermodynamics within the eruption column and in the ambient atmosphere during eruption and shortly afterward. ATHAM considers cloud microphysics for liquid and frozen hydrometeors as well as aggregation of volcanic particles. We focus on the investigation of the fate of the fine fraction in the atmosphere. The ATHAM model is described in more detail in a companion paper (Textor et al., 2005—this issue) hereafter referred to as Paper II. Here we discuss the microphysics of hydrometeors and ash particles within the eruption column and the parameterizations

employed in the ATHAM model. In the next section, we introduce the nomenclature and abbreviations used throughout this study. We describe the fate of volcanic particles within the eruption column in Section 3. Section 4 presents the microphysical processes of hydrometeors and ash particles. In this section we explain our parameterization to simulate these processes, and in Section 5 we discuss the advantages and limitations of our approach. An analysis of various factors that influence aggregation of volcanic particles based on numerical experiments with the ATHAM model employing these parameterizations is performed in Paper II.

2. Nomenclature

In the context of this study, we distinguish between 'ash', 'hydrometeors' and 'aggregates'. The first refers to pure volcanic particles. The term 'hydrometeor' denotes any product of condensation of liquid water or deposition of ice of water vapor in the atmosphere (clouds and precipitation). For a comprehensive description of the properties of hydrometeors see Pruppacher and Klett (1997). Clusters of ash and hydrometeors are called aggregates. 'Particles' is used to signify any of these three types. Table 1 provides the definitions of the indices, variables and terms used in this paper and in Paper II.

3. Particles in the eruption column

Excellent summaries of the processes occurring during volcanic eruptions are provided for example by Sparks et al. (1997) or with a special focus on volcanic ash in the atmosphere by Bursik (1998). Here, we give a short overview on those processes that are relevant for particle aggregation during so-called Plinian eruptions. These are characterized by mass eruption rates of the order of 10^8 kg s^{-1} during several hours. During the ascent of magma from the magma chamber decompression leads to the exsolution of dissolved gases. This produces an overpressured magmatic foam that accelerates upwards. Typically, several hundred meters below the vent the increasing gas volume fraction results in fragmentation thus generating a particle-loaded gas with increased vertical velocity. Plinian eruptions are most often caused by high-viscosity magma (andesitic or rhyolitic) with large contents of Silica SiO_2 (>50 wt.%) and several weight percents of volatiles. A multiphase, overpressured and upward-directed, negatively buoyant, momentum-dominated jet exits the vent, which is some

Table 1
Definition of the indices, variables and terms used throughout this paper and in Paper II

Variable	Meaning
ϵ	Relevant ratio of hydrometeor and ash for collection efficiency
v	Skewness parameter of the gamma function
$\bar{r}$	Radius of average mass [m]
Γ	Gamma function
ρ	Density [kg m^{-3}]
C_D	Drag coefficient
CCN	Cloud condensation nuclei
E	Collection efficiency
F_{gam}	Normalized gamma function
HNB	Height of neutral buoyancy [km]
IN	Ice nuclei
M	Average mass of a single particle [kg]
N	Number concentration [number kg^{-1}] in relation to total mass in the grid box
P	Moment of the gamma function
T	Temperature in [K] if not otherwise indicated
T_0	Freezing temperature T_0=273.15 K (without salinity effects)
acc	Accretion
aut	Autoconversion
ax	Ash in category x
c	index for small warm ash/cloud water
c_{aut}	See Section 4.6.2
coal	Coalescence
c_s	Speed of sound
c_p	Specific heat capacity at constant pressure
c_v	Specific heat capacity at constant volume
colli	Collision
e	Air or gas phase
$e0$	Air at sea level
f	Fraction of ash or hydrometeor in an aggregate
g	index for large cold ash/groupel
grav	Gravitational constant, grav ≈ 9.81 [m s^{-2}]
h	Water vapor
i	index for small cold ash/cloud ice
k	Constants in the fall velocity equations, units in the text
l	Large
m	Mass [kg s^{-1}]
$\dot{M}$	Mass eruption rate [kg s^{-1}]
mix	Gas–particle mixture [kg]
nuc	Nucleation
nucmax	Maximum number concentration for nucleation
p	index for large warm ash/rain
px	Particle in category x
q	Mass mixing ratio [kg kg^{-1}] in relation to total mass in the grid box
rad	Radius of the eruption column base [m]
r	Particle radius [m]
r_{mode}	Modal particle radius [m]
r_n	Characteristic particle radius [m]
s	Small
t	Time [s]
Δt	Model time step (typically 0.5 s in ATHAM)
w	Terminal fall velocity [m s^{-1}]
w_b	Vertical velocity at eruption column base [m s^{-1}]
x	Hydrometeor in category x

All quantities are given in SI-units.

tens of meters in diameter, at the speed of sound. The density of the multiphase flow is typically 5–50 times denser than surrounding air. The near-surface vent geometry strongly influences the speed of the decompressing mixture and can result in supersonic or subsonic flows. Adjustment to atmospheric pressure takes place during the first 1–100 s and a few jet radii above the vent. The flow speed at the eruption column base can be at most twice the speed of sound, if the apex angle of the crater is wide enough (Woods and Bower, 1995).

The exiting gas particle mixture is characterized by vertical velocities of the order of some 100–500 m s^{-1} and temperatures of 1000–1400 K. The composition of volcanic ash varies from one volcano to another. Apart from silica it consists of smaller amounts of the oxides of aluminum, iron, calcium and sodium. The silica particles are mainly in the form of sharp-edged glass shards. The density of volcanic juvenile particles depends on the mechanism of their formation. It can vary from magmatic density (2600 kg/m^3) to highly vesicular pumice (500 kg/m^3). For individual volcanic particles between 30 and 500 μm, Wilson and Huang (1979) found a density range of 800–2650 kg/m^3. The size of the particles depends on the conditions in the magma, and is strongly linked to the fragmentation process (e.g., Kaminski and Jaupart, 1998). The size distributions of volcanic particles are inferred from large sedimentological data sets, which are believed to reflect the original particle distribution at the volcanic vent. This assumption is only justified if particle aggregates, which form in the eruption column disaggregate upon impact with the ground or during the sample collection. It is not possible to determine to what extent the erupted particles have been modified before data evaluation. Woods and Bursik (1991) and Bursik (1998) present typical size distributions inferred for different eruption types. The effect of different erupted size distributions on the plume microphysics and geometry is the subject of a sensitivity study with the ATHAM model in Paper II. The gas fraction in the erupting mixture typically is 3–5 wt.%, where water vapor is with 50–90% the dominant component, followed by carbon dioxide (1–40%), sulfur dioxide (1–25%), hydrogen sulfide (1–10%), and hydrogen chloride (1–10%), and trace gases (e.g., Symonds et al., 1988). The strong temperature decrease can lead to crystallization of metal salts both nucleating new particles or on existing ash surfaces.

The density of the erupted mixture after adjustment to ambient pressure is still higher than that of the ambient atmosphere. Upwards movement the lowest few kilometers above the vent in the so-called gas-thrust region is due to the initial momentum. Dilution by entrainment of air, rapid heat exchange between pyroclasts and entrained air and further expansion can generate a buoyant eruption column. Vertical velocities in Plinian columns are of the order of some hundreds of meters per second depending on the volcanological and environmental conditions, i.e., one order of magnitude greater than in thunderstorm clouds. Such eruption columns ascend within less than 10 min from the ground to the stratosphere. Initial temperatures are very high in the column core with strong cooling towards the fringes.

As soon as the saturation pressure of water vapor is reached, liquid water condensation or ice deposition takes place. Water vapor originates from the magma, from entrained air and sometimes from external ground- or seawater, and thus varies strongly from one eruption to another. The cloud condensation level is at much higher altitudes than in usual convective clouds. Due to the great height of the umbrella region, most of the hydrometeors freeze during ascent. To our knowledge no direct observational data of the physical state or of the composition of hydrometeors exist for Plinian eruptions. Recent satellite observations of ash clouds however provide strong indirect evidence that ice is present on ash particles (Rose et al. 1995, 2003; Mayberry et al., 2003; Lacasse et al., 2004; Guo et al., 2004a,b). These data are based on the method of Wen and Rose (1994), that causes to discriminate volcanic silicate particles and hydrometeors in IR satellite data (e.g., AVHRR) based on the sign of the brightness temperature difference between the thermal infrared bands. With this technique, ash particles with a sufficiently thick ice cover appear as pure ice particles, and those with a low ice fraction may show ash silicate IR signals. The role of water and ice in volcanic eruption columns still needs to be clarified. The presence of soluble gases and of soluble salts coating ash particles (e.g., Rose, 1977; Rose et al., 1982; Smith et al., 1982; Varekamp et al., 1986) could cause a depression of the saturation pressure and shift the freezing point to lower temperatures (salinity effect). Please note that the amount of sulfuric acid in the eruption column shortly after eruption is probably not significant when compared to other soluble species. The direct eruption of sulfate is small, and oxidation of its precursor gases (SO_2 and H_2S) does not take place to a large degree during plume rise. This is due to the short rise time, and to the lack of photo-oxidants within the opaque plume (Textor et al., 2003b). The number concentration of particles in a

volcanic plume is extremely high. Particle concentrations are at least three orders of magnitude greater than in continental meteorological clouds. Hobbs et al. (1982) reported the number of ash particles at the periphery of the Mt. St. Helens plume to be 20,000 times greater than in the ambient air. Thus, supersaturation is most likely to be removed by water vapor condensation on ash particles, which act as cloud water condensation nuclei (CCN) and ice nuclei (IN). Ash particles are mostly larger than 1 μm in radius, and often coated with hygroscopic salt crystals. This makes ash suitable for initiating water drops from water vapor. Although there is still some controversy about the capacity of volcanic ash particles to act as IN, they have been observed to exhibit a large nucleating ability (e.g., Isono et al., 1959; Schnell and Delany, 1976; Shaw et al., 2005). For an overview on particle nucleating abilities see Pruppacher and Klett (1997). The nucleation processes cannot be resolved by satellite observations, and in-situ measurements in ash clouds as well as laboratory experiments are needed.

A buoyancy-driven convective column of Plinian type reaches heights of neutral buoyancy (HNB) at some tens of kilometers altitude (i.e., in the stratosphere), where its density converges to that of the ambient fluid. The potential energy at that height is equal to the erupted kinetic and thermal energy (the latter is typically 10 to 100 times larger than the former), and the latent heat gained from water vapor condensation within the plume. The diameter of a Plinian column in the region below the HNB is 10–20 km. An either radial or parabolically shaped umbrella cloud with a thickness of some kilometers is generated depending on the plume size and the wind conditions. The plume's inertia can lead to overshooting above HNB by several kilometers. The material falls back generating gravity waves. Umbrella clouds from Plinian eruptions expand horizontally in the stratosphere as gravity intrusions modified by the local wind. The expansion of the Pinatubo cloud on June 15, 1991 took place at a radial velocity of about 125 m s^{-1}, the umbrella had a diameter of about 400 km after 1 h. Volcanic ash particles are rather quickly removed from the atmosphere by sedimentation within the first hours to days after eruption, especially when aggregates are formed. The fallout of volcanic ash can cover areas of several thousands of kilometers. In the months following a Plinian eruption sulfur-containing gases are oxidized to sulfate aerosol particles in the stratosphere. These can affect the global climate on time scales of months to years.

Ash aggregates or indirect evidence for them have been found in several recent volcanic deposits (e.g., Sorem, 1982; Carey and Sigurdsson, 1982 at Mt. St. Helens, Mackinnon et al., 1984 at El Chichón, Wiesner et al., 1995 at Mt. Pinatubo, or Bonadonna et al., 2002a at Soufriere Hills of Montserrat). Well-preserved aggregates are also common in the geological record in ash layers laid down during phreatomagmatic eruptions (e.g., Self and Sparks, 1978; Schumacher and Schmincke, 1991; Durant and Ernst, submitted for publication). Despite some insightful experimental studies (Lane et al., 1993; Gilbert and Lane, 1994; Schumacher, 1994; James et al., 2000, 2002, 2003) the formation processes of ash aggregates inside the eruption column remain incompletely understood. Ash clusters are porous, especially when they are dry, and non-spherical in shape (e.g., Sorem, 1982). In addition, posteruptive processes might alter aggregates after emplacement on the ground (e.g., Durant et al., 2002). Particle density and shape strongly influence the aerodynamic fall behavior (Walker et al., 1971; Wilson and Huang, 1979; Lane et al., 1993; Riley et al., 2003). A profound knowledge of the particle qualities and modification processes during and after eruption is relevant for studies of ash and SO_2 dispersal by explosive eruptions (e.g., Carey and Sigurdsson, 1982; Rose et al., 1982, 2000, 2001; Textor, 1999; Textor et al., 2003a,b).

Aggregates of volcanic particles can be divided in three main classes: dry aggregates, accretionary lapilli and mud rain. The in-cloud abundance of a specific type depends on the amount of water available during aggregation (Gilbert and Lane, 1994; Schumacher and Schmincke, 1995; Sparks et al., 1997). Particle collisions within volcanic eruption columns are mainly caused by differences in their terminal fall velocities, because volcanic particles and hydrometeors are in the 1–1000 μm size range and of different dimensions, as discussed in detail by Textor and Ernst (2004). This process of gravitational collection can be enhanced by turbulent motions and by electrostatic forces. Especially for fine charged particles built of dry, non-conductive material it has been hypothesized that electrostatic attraction is effective in comparatively dry environments (for references see Sparks et al., 1997) when other forces are less relevant. Quantitative observations on the role of electrostatic forces in particle aggregation processes are rather incomplete at the moment but some important papers have been published (Gilbert and Lane, 1994; Schumacher, 1994; James et al., 2000, 2002, 2003). The generation of charged particles is due to fracturing of magma already in the conduit,

and continues into the jet region and onwards until charge can dissipate when the particles land on the ground (e.g., Lane and Gilbert, 1992). Electric charge resides on the particle surfaces. Fine ashes have larger charge-to-mass-ratios because of their larger surface-to-volume-ratios and are therefore more likely to aggregate due to electrostatic forces (Gilbert et al., 1991). As soon as charged particles are generated, electrostatic aggregation processes take place.

Once ash particles have collided, they need to bind (coalesce, stick together) to form aggregates. It seems that for dry particles electrostatic or van-der-Waals-forces lead to successful coalescence, although such dry aggregates are weakly bound and readily collapse upon landing on the ground. If water is available, much stronger particle bonds result from short-range surface tension forces. Volcanic particles become moist by water vapor condensation on their surfaces or by collision with wet particles. The presence of dissolved salts establishes more durable particle contacts when evaporation leads to enhanced concentrations finally resulting in crystal bridges that greatly increase the strength of the inter-particle bonds (Gilbert and Lane, 1994). This process is referred to as 'cementation'. Preservation of frozen aggregates is expected to arise both from the presence of a soft ash matrix which is largely impermeable and from the difficulty for water within melting aggregates to drain out of narrow pores ($\sim$ 10 μm scale). In addition to the clustering mechanisms mentioned above, Sorem (1982) suggested that geometrical interlocking of dry particles of irregular shape may bind particles as in snow flakes. Reversible binding forces, aerodynamic resistance during fallout, or impact on the ground may lead to aggregate breakup (e.g., Durant and Ernst, submitted for publication).

In the frame of this study, we assume gravitational capture is the main mechanism leading to particle collisions and neglect less important other processes. Here, aggregation is exclusively caused by interaction between volcanic ash and hydrometeors within the eruption column. Bonding depends on the amount of hydrometeor on the particle surface, as explained in the next section. We also show a first estimation for the relevance of aggregation of dry ash particles caused by electrostatic forces in Paper II.

4. Parameterization of the microphysics of hydrometeors and ash

A new parameterization has been developed in the framework of this study. The older, extended Kessler-type parameterization employed in the previous version of ATHAM (Herzog et al., 1998; Graf et al., 1999) described the microphysics of hydrometeors based on their mass mixing ratios. The new scheme is a modal approach, and two moments of the distribution, the mass mixing ratio and the number concentration, are explicitly calculated as prognostic variables following Walko et al. (1995) and Meyers et al. (1997). The particle size distributions are described with gamma functions as proposed by Flatau et al. (1989). In addition to hydrometeors, we consider the microphysics of volcanic ash. Interactions between hydrometeors and volcanic ash lead to particle aggregation. Our microphysical formulation is based on the microphysical concept for usual atmospheric ('meteorological') clouds with the extension that volcanic particles can be contained in all categories of hydrometeors forming mixed hydrometeor–ash particles. This new concept is analogous to the approach of Molenkamp and Bradley (1990) for aerosol scavenging in smoke plumes or meteorological clouds. Ash particles sufficiently coated with water or ice act in a similar microphysical manner as pure hydrometeors with minor changes according to the relative mass fraction of ash and hydrometeors as described hereafter. This is intuitively justified by the fact that two water-coated ash particles will 'see' each other as two liquid drops if the amount of water at the particle's surface is sufficient.

4.1. Simulated categories of hydrometeors and volcanic ashes

Following common approaches for bulk parameterizations of cloud microphysics, we describe the hydrometeors by two size classes (modes). One consists of larger particles that settle under gravity and the other of smaller particles that are rather suspended in the air. Each of these size classes is subdivided into a frozen and a liquid category. The larger hydrometeors are called 'rain' for liquid water and 'graupel' for the frozen category. The name 'graupel' is chosen fairly arbitrarily for a category of intermediate-density, frozen hydrometeors. By analogy with the hydrometeor classification we specify two size classes of volcanic ash particles, each with a warm and a cold category. Apart from water vapor, we thus consider the mass mixing ratios q of four categories x of hydrometeors and four categories ax of ash as prognostic variables. As ash and hydrometeors coexist at a given grid point, we assume that they are contained in mixed aggregates. The composition of these aggregates is given

Table 2
Particle categories considered in ATHAM with the characteristics given in the left column

Characteristics	Index	Hydrometeor	Ash	Mixed particles
Small warm	c	Cloud water	Small ash $T>T_0$	Ash/water
Small cold	i	Cloud ice	Small ash $T<T_0$	Ash/ice
Large warm	p	Rain	Large ash $T>T_0$	Ash/water
Large cold	g	Graupel	Large ash $T<T_0$	Ash/ice

The second column refers to pure hydrometeors, the third to pure ash, and the right to mixed hydrometeor–ash particles. T_0 is the freezing temperature.

by the sum of the mass mixing ratios of ash and hydrometeors:

$$q_{px} = q_x + q_{ax}. \quad (1)$$

These particles p_x can either be dry ash, pure hydrometeors or mixed hydrometeor–ash particles (aggregates), depending on the relative concentration of ash and hydrometeor given in Eq. (1). The concept of Gilbert and Lane (1994) of wet ash or mud rain is included in our parameterization. The number concentrations N of the particles in the four categories p_x are prognostic variables. Table 2 gives an overview of the particle categories, see also Fig. 1.

In ATHAM, volcanic ash erupted at the vent is initialized in the two warm categories c and p. The size distribution is represented by the superposition of the two modes. (In our reference experiment, the radii of average mass of the small and large category are 2.5 μm and 50 μm, respectively, see Paper II.) As soon as the temperature in the rising eruption column falls below the freezing level, pure volcanic ash is reclassified to the corresponding cold categories i and g. If the ash is contained in mixed hydrometeor–ash aggregates, it undergoes the same microphysical processes as hydrometeors. This means, for example, that freezing of water to ice in a mixed particle also transfers warm ash to the respective cold ash category.

The density of mixed hydrometeor–ash particles ρ_{px} is obtained from the volume ratio of ash and water:

$$\rho_{px} = \frac{q_x + q_{ax}}{q_x/\rho_x + q_{ax}/\rho_{ax}}. \quad (2)$$

For example, a mixed particle composed of water and ash in equal shares by mass with individual densities of 1000 and 1800 kg/m^3 would have a density of 1286 kg/m^3. This is in the range of densities found for mud rain (Sparks et al., 1997; Durant and Ernst, submitted for publication). A relation of 10 wt.% water and 90 wt.% ash would lead to an aggregate density of 1700 kg/m^3, more typical for dense accretionary lapilli (Sparks et al., 1997). Like all other qualities of mixed particles, the density also converges to that of the pure

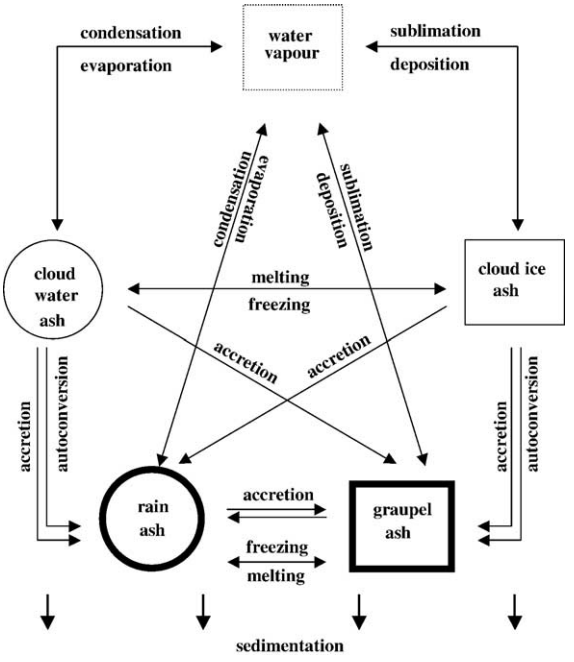

Fig. 1. Reprensentation of the microphysical processes within an eruption column in the ATHAM-model. Circles: warm categories; squares: cold categories; dotted lines: gas; thin lines: small categories; bold lines: large categories.

material in the absence of the other phase. We neglect in this first study for simplicity the possibility of any air bubbles within the aggregates, which would reduce their density.

4.2. Representation of size distributions

In our modal microphysical parameterization the size distribution of each mode is assumed to follow a generalized gamma function $F_{\mathrm{gam}}(r_{px})$, an empirical function often used in cloud microphysics (e.g., Flatau et al., 1989; Verlinde et al., 1990; Walko et al., 1995). The generalized gamma distribution $F_{\mathrm{gam}}(r_{px})$ is given by:

$$F_{\mathrm{gam}}\left(r_{px}\right) = \frac{1}{\Gamma\left(\nu_{px}\right)}\left(\frac{r_{px}}{r_{n,px}}\right)^{\nu_{px}-1}\frac{1}{r_{n,px}}\exp\left(-\frac{r_{px}}{r_{n,px}}\right). \tag{3}$$

$F_{\mathrm{gam}}(r_{px})$ is the probability to find a particle of a certain radius r_{px}. ν_{px} is the dimensionless skewness parameter of the size distribution. $\Gamma(\nu_{px})$ is the gamma function of ν_{px}, which serves as a normalization constant to make the complete integral of $F_{\mathrm{gam}}(r_{px})$ with respect to r_{px} equal to 1. The characteristic radius $r_{n,px}$ helps normalizing r_{px} to ensure that the exponent is a non-dimensional number. It is dependent on the mass mixing ratio q_{px} and on the total number concentration N_{px} of the particles p_x with the density ρ_{px}:

$$r_{n,px} = \left(\frac{q_{px}}{N_{px}}\frac{3}{4\pi\rho_{px}}\frac{\Gamma\left(\nu_{px}\right)}{\Gamma\left(\nu_{px}+3\right)}\right)^{\frac{1}{3}}. \tag{4}$$

$r_{n,px}$ is related to the modal radius r_{mode}, which is the most frequent radius of the particle size distribution (Seinfeld and Pandis, 1997):

$$r_{\mathrm{mode}} = \left(\nu_{px}-1\right)r_{n,px}. \tag{5}$$

The distribution of the number concentration $N(r_{px})$ is described by multiplying the generalized gamma function with the total particle number N_{px}:

$$N\left(r_{px}\right) = N_{px}F_{\mathrm{gam}}\left(r_{px}\right), \tag{6}$$

and the mass distribution m (r_{px}), can be derived from

$$m\left(r_{px}\right) = N\left(r_{px}\right)\frac{4}{3}\pi r_{px}^{3}\rho_{px} = N_{px}\frac{4}{3}\pi r_{px}^{3}\rho_{px}F_{\mathrm{gam}}\left(r_{px}\right). \tag{7}$$

The skewnesses of the distributions are prescribed in our study as described below. Thus the size distributions $N(r_{px})$ and $m(r_{px})$ for each particle class can be analytically derived from q_{px} and N_{px}, which are explicitly calculated as prognostic variables during the model runs.

The advantage of using generalized gamma functions is that an analytical solution for the complete integral can be obtained for any of its moments P. This is useful to solve the equations for the aggregation process, see Section 4.6.1. The values of ν_{px}, $\Gamma(\nu_{px})$ and $r_{n,px}$ are constant at a given grid point during one model time step of the numerical experiment and we get:

$$\int_0^\infty r_{px}^{P}F_{\mathrm{gam}}\left(r_{px}\right)\mathrm{d}r_{px} = r_{n,px}^{P}\frac{\Gamma\left(\nu_{px}+P\right)}{\Gamma\left(\nu_{px}\right)}. \tag{8}$$

The results of the integrations of Eq. (6) where $P=0$, or Eq. (7) where $P=3$, are used to derive the number concentration, and the mass mixing ratio, respectively.

The selection of the skewness parameters is rather difficult, since not many observations of size distributions are available, especially not for particles in volcanic eruption columns. We take $\nu_r=\nu_g=3.5$, as observed by Willis (1984) for rain in usual meteorological clouds. Because of the lack of information about ice particle qualities, and for simplicity, the same skewness parameter is applied for graupel. The size distributions of cloud water and cloud ice are described with $\nu_c=\nu_i=16$ as used by Beheng and Doms (1990) and Lüpkes (1991) for typical continental clouds with high concentrations of condensation nuclei. We also expect to get narrow, rather symmetrical distributions in an eruption column due to the presence of many condensation nuclei provided by the ash particles. The skewness parameters of the size distributions of mixed hydrometeor–ash particles, ν_{px}, should be dependent on the formation process and on relative mass fractions of hydrometeors and ash. Because no observational data exist, it is obtained here from linear interpolation with respect to the mass fraction of ash and water in this study:

$$\nu_{px} = \frac{q_{ax}\nu_{ax}+q_x\nu_x}{q_{ax}+q_x} \tag{9}$$

4.3. Description of terminal fall velocities

We consider the fall velocity of each particle class in our model concept. The terminal velocities of the particles are estimated as described in Herzog et al. (1998), using the particle densities given in Eq. (2). For particles of the order of 50 μm in radius, the relative motion between gas and particles can be described by Stokes law: the friction force is proportional to the relative particle velocity. The terminal fall velocity of an individual particle w_1 is then proportional to the square of

the particle radius $\bar{r}_{px}$ (Rogers and Yau, 1989). We use the radius of average mass r_{px}, since the fall velocity is determined by the particle mass:

$$w_1(r_{px}) = k_1 \rho_{px} \sqrt{\frac{\rho_{e0}}{\rho_e}} \bar{r}_{px}^2 \tag{10}$$

where $k_1 = 1.19 \times 10^5$ m^2 kg^{-1} s^{-1}. The density factor $\sqrt{\rho_{e0}/\rho_e}$ accounts for the increase of the fall velocity with height. ρ_{e0} is the air density at sea level and ρ_e is the air density at the particle height.

For medium size particles with radii between about 50 μm and 500 μm, the fall velocity increases approximately linearly with the radius (Rogers and Yau, 1989):

$$w_2(r_{px}) = k_2 \rho_{px} \sqrt{\frac{\rho_{e0}}{\rho_e}} \bar{r}_{px} \tag{11}$$

where $k_2 = 8$ m^3 kg^{-1} s^{-1}.

Large particles ($r_{px} > 500$ μm) are influenced by Newtonian friction which is proportional to the square of the particle velocity. The terminal fall velocity is proportional to the square root of the particle radius (Rogers and Yau, 1989):

$$w_3(r_{px}) = \sqrt{\frac{8}{3} \frac{\rho_{px} \mathrm{grav}}{c_{D,x} \rho_{e0}}} \sqrt{\frac{\rho_{e0}}{\rho_e}} \sqrt{\bar{r}_{px}} = k_3 \sqrt{\frac{\rho_{px}}{C_{D,x}}} \sqrt{\frac{\rho_{e0}}{\rho_e}} \sqrt{\bar{r}_{px}} \tag{12}$$

where $k_3 = 4.833$ m^2 s^{-1} kg$^{-1/2}$, grav $= 9.81$ m s^{-2} is the gravitational constant.

The drag coefficient, $C_{D,x}$, is a parameter accounting for the particles' surface roughness. For water droplets we use a value of 0.54 as determined by Gunn and Kinzer (1949). For frozen hydrometeors we take 0.6 as assumed for graupel by Wisner et al. (1972). The drag coefficients for ash of different shapes and dimensions have not been explicitly measured. We use a value of 0.75 as employed by Carey and Sparks (1986) and Armienti et al. (1988) to simulate the settling velocity behavior of volcanic particles measured by Walker et al. (1971) and Wilson and Huang (1979). The weak dependence on flow characteristics and particle size is neglected. For hydrometeor–ash aggregates we interpolate linearly between the values for hydrometeor and ash, dependent on their relative mass mixing ratios. Aggregates have a larger fall velocity than the individual particles due to their larger size (e.g., Lane et al., 1993).

Our formulation takes into account the effects of particle density, size, surface roughness, and the effect of decreasing friction with height in the atmosphere as explained in Herzog et al. (1998).

4.4. Microphysical processes considered in the model

The microphysical processes in our parameterization depend on mass mixing ratio, radius and number concentration of particles that can be pure hydrometeors, pure volcanic ash or mixed hydrometeor–ash particles. A schematic representation of the microphysical framework is illustrated in Fig. 1 and explained in the following sections.

Mixed hydrometeor–ash particles of any contribution of water, ice and volcanic ash take part in the processes. Here, as a first approximation, it is assumed that the ash aggregates are internally well mixed, i.e., they have the same composition within a volume represented by a given grid point. The individual mass transfers of the components are calculated in proportion to their fraction f in the aggregates:

$$f_x = \frac{q_x}{q_{px}} \text{ and } f_{ax} = 1 - f_x, \tag{13}$$

$$\frac{\partial}{\partial t} q_x = f_x \frac{\partial}{\partial t} q_{px} \tag{14}$$

and

$$\frac{\partial}{\partial t} q_{ax} = f_{ax} \frac{\partial}{\partial t} q_{px}. \tag{15}$$

All microphysical processes that include a phase change of water consume or produce thermal energy, this way influencing the dynamics of the entire system as described in Herzog et al. (1998). A balance procedure ensures that the phase transfer of water vapor is confined to the existing super- or sub-saturation and guarantees mass conservation.

The influences of dissolved species on the thermodynamic properties of the water (salinity effect) are examined in sensitivity studies presented in Paper II. Since information on the composition of the particles within volcanic eruption columns is very limited at the moment, we employ the simple parameterizations based on the concentration of dissolved volcanic gases as discussed in Textor et al. (2003a).

4.5. Water vapor transfer processes

Once supersaturation is reached in the rising eruption column, water vapor starts to condense and forms liquid water or ice at existing ash particles. In this study, we do not explicitly consider this heterogeneous nucleation process, but assume that dry ash is able to

grow by water vapor condensation or deposition in just the same way that droplets do, see the discussion in Section 3. We examine the sensitivity of the eruption column development to different temperature dependencies of ice nucleation in a numerical experiment in Paper II. The formulation of water vapor transfer processes (condensation at and evaporation of liquid droplets, as well as deposition at and sublimation of ice particles) in ATHAM has been described in Herzog et al. (1998), it is based on the approach of Byers (1965). Water vapor transfer for mixed hydrometeor–ash aggregates is treated in an analogous way to that of pure hydrometeors assuming that the water or ice is situated at the aggregate's surface. The ash content and the number concentration are not changed during water vapor transfer.

Hydrometeor nucleation on non-volcanic particles, or even homogeneous nucleation is highly unlikely within the volcanic eruption column. To account for hydrometeor nucleation outside the eruption column in the background atmosphere we have implemented a simple nucleation parameterization in ATHAM. Twomey and Wojciechowski (1969) provide an empirical function for the dependency of the CCN number concentration on water supersaturation in continental air as a function of:

$$N_{\mathrm{nucmax,c}} = 6 \cdot 10^8 \sqrt{S_{\mathrm{w}} - 1} \tag{16}$$

where the saturation ratio $S_{\mathrm{w}} = q_{\mathrm{h}}/q_{\mathrm{sat,w}}$ is the ratio of the mass mixing ratios of the water vapor present q_{h} and of the theoretical saturation value with respect to liquid water $q_{\mathrm{sat,w}}$. In our simulations, new cloud drops are nucleated until $N_{\mathrm{nucmax,c}}$ is reached, but only if water vapor saturation has not already been attained by condensation on existing particles. The change in mass mixing ratio of cloud water is obtained from multiplication with the mass of a single nucleated particle $m_{\mathrm{nuc,c}}$:

$$\left.\frac{\partial}{\partial t} q_{\mathrm{c}}\right|_{\mathrm{nuc}} = -\left.\frac{\partial}{\partial t} q_{\mathrm{h}}\right|_{\mathrm{nuc}} = \min\left(\left(N_{\mathrm{nucmax}} - N_{\mathrm{p}}\right) \cdot m_{\mathrm{nuc}}, \frac{q_{\mathrm{h}} - q_{\mathrm{sat,w}}}{\Delta t}\right). \tag{17}$$

The radius of nucleated cloud droplets in the background atmosphere is set constant to 0.1 μm. We follow an analogous approach for the nucleation of cloud ice particles in the undisturbed atmosphere. The number of active ice nuclei IN depends on the temperature (Fletcher, 1962):

$$N_{\mathrm{nucmax},i} = \frac{q_e}{\rho_e} N_{0,f} \exp(\beta(T_0 - T)) \tag{18}$$

with

$$\beta = 0.6K^{-1} \text{ and } N_{0,f} = 10^{-2}\ \mathrm{m}^{-3}.$$

β and $N_{0,f}$ are empirical constants, and $T_0 = 273.15$ °C is the freezing temperature. The exponential decrease of IN with increasing temperature causes this process to be only significant at temperatures well below freezing point. We prescribe a radius of 0.1 μm for the nucleated ice crystals in the background atmosphere.

Please note that these nucleation parameterizations are entirely insignificant inside the eruption column where water vapor condenses on abundant ash particles.

4.6. Aggregation

Aggregation is described by two processes in our model. We have to distinguish between inter- and intramodal aggregation, because of the simplified representations of the size distributions, see Section 4.2. Intermodal aggregation due to gravitational capture among particles in modes of different sizes is called 'accretion' in cloud microphysics. This process leads to a gain of particles in the larger mode at the expense of the smaller one, see Section 4.6.1. Accretion among all modes of different sizes and thus different fall velocities are accounted for in ATHAM. Intramodal aggregation within one size class is tagged 'autoconversion'. This process cannot be explicitly calculated, it has to be parameterized, see Section 4.6.2. Table 3 summarizes the aggregation processes considered in ATHAM.

4.6.1. Accretion

Large particles l capture all small particles s inside a swept volume, which is determined by par-

Table 3
Aggregation processes considered in ATHAM

Collecting category	Collected category	Destination category
Large warm	Small warm	Large warm
Large warm	Small cold	Large warm if $T > T_0$
Large warm	Small cold	Large cold if $T < T_0$
Small cold	Large warm	Large cold if $T < T_0$
Large cold	Small cold	Large cold
Large cold	Small warm	Large cold if $T < T_0$
Large cold	Small warm	Large cold melting if $T > T_0$
Large cold	Large warm	Large cold if $T < T_0$
Large cold	Large warm	Large warm if $T > T_0$
Small warm	Small warm	Large warm
Small cold	Small cold	Large cold
Large cold	Large cold	Large cold

The first 9 processes are due to accretion and the last three to autoconversion, see text. For the particle categories in ATHAM see Table 2.

ticle radii r and the difference in fall velocities w: $\pi(r_s+r_l)^2|w_s(r_s)+w_l(r_l)|$ (see also Sparks et al., 1997, p. 445). The rate at which the number concentration N of small particles decreases is given by the stochastic collection equation (e.g., Pruppacher and Klett, 1997):

$$\left.\frac{\partial N_s}{\partial t}\right|_{\text{acc}} = -\frac{\rho_e}{q_e}\pi E\int_0^\infty\int_0^\infty \pi(r_s+r_l)^2 \\ |w_s(r_s)+w_l(r_l)|N_s(r_s)\mathrm{d}r_s N_l(r_l)\mathrm{d}r_l \qquad (19)$$

where E is the collection efficiency for accretion (see Section 4.7). The ratio of the density and the mass mixing ratio of air ρ_e/q_e converts the units of right hand side of Eq. (19) from numbers per volume to numbers per total mass per unit time.

The corresponding rate of change in the mass mixing ratio of small particles may be written as:

$$\left.\frac{\partial q_s}{\partial t}\right|_{\text{acc}} = -\frac{\rho_e}{q_e}\frac{4}{3}\pi^2\rho_s E\int_0^\infty\int_0^\infty \pi(r_s+r_l)^2 \\ |w_s(r_s)+w_l(r_l)|N_s(r_s)\mathrm{d}r_s N_l(r_l)\mathrm{d}r_l. \qquad (20)$$

This mass is gained by the larger, collecting particles. Their number does not change, they therefore grow in size. The analytical solution of these double integrals is difficult to obtain without further assumptions, as discussed by Verlinde et al. (1990). In this study we use for the difference of terminal fall velocities $w_s(r_s)-w_l(r_l)$ in Eqs. (19) and (20) the constant value Δw_{ls} calculated for the radii of average mass of the distributions, which can be drawn out of the integral according to Wisner et al. (1972). The general solution of these equations can be obtained analytically with the aid of Eq. (8):

$$\left.\frac{\partial N_s}{\partial t}\right|_{\text{acc}} = -\frac{\rho_e}{q_e}\pi E|\Delta w_{ls}|\frac{1}{\Gamma(\nu_s)\Gamma(\nu_l)} \\ \cdot(N_s r_{n,s}^2\Gamma(\nu_s+2)\Gamma(\nu_l) \\ +2N_s r_{n,s}\Gamma(\nu_s+1)N_l r_{n,l}\Gamma(\nu_l+1) \\ +N_l r_{n,1}^2\Gamma(\nu_1+2)\Gamma(\nu_s)). \qquad (21)$$

$$\left.\frac{\partial q_s}{\partial t}\right|_{\text{acc}} = -\frac{\rho_e}{q_e}\frac{4}{3}\pi^2\rho_s E|\Delta w_{ls}|\frac{1}{\Gamma(\nu_s)\Gamma(\nu_l)} \\ \cdot(N_s r_{n,s}^5\Gamma(\nu_s+5)\Gamma(\nu_l) \\ +2N_s r_{n,s}^4\Gamma(\nu_s+4)N_l r_{n,l}\Gamma(\nu_l+1) \\ +N_s r_{n,s}^3\Gamma(\nu_s+3)N_l r_{n,l}^2\Gamma(\nu_l+2)). \qquad (22)$$

The respective changes of the hydrometeor and ash contents within aggregates are calculated from Eqs. (14) and (15). Below the freezing level, accretion of the small cold category (cloud ice/ash) by the large warm category (rain/ash) leads to contact-freezing of supercooled water forming large cold particles (graupel/ash). The destination category is different from both the collecting and the collected category. In this case, the accretion process is calculated twice with the collector and collecting categories reversed, to account for the losses of the two participating categories. Accretion of warm small particles (cloud water/ash) by large cold ones (graupel/ash) at temperatures below freezing leads to contact-freezing of the warm small particles (cloud water/ash) increasing the mass in the large cold category. Above the freezing point, melting graupel in the large cold category and accretioned cloud droplets in the warm small category form new rain water pertaining to the large warm category, transferring any ash with them among these categories. Accretion of large cold (graupel/ash) and large warm particles (rain/ash) leads to more large cold particles (graupel/ash) below the freezing temperature. At warmer temperatures melting graupel in the large cold category collecting large warm particles (rain/ash) drops adds to the amount of the latter category. The gain of heat from melting graupel resulting in additional melting is considered in the melting equation as described in Herzog et al. (1998).

4.6.2. Autoconversion

Several concepts for the autoconversion rate exist for meteorological clouds which depend both on the mass mixing ratio and on the particle size, e.g., Berry and Reinhardt (1974) or Beheng (1994). However, these approaches implicitly assume a threshold radius for the transition from the smaller to the larger category of 40 μm. This assumption cannot be applied in our concept in the presence of ash where the threshold radius $\bar{r}_{l0}$ is given by the radius of the larger ash class. We therefore use a parameterization similar to that of Murakami (1990), which explicitly allows for modifications of the threshold radius. The rate of collision–coalescence due to gravitational capture within a homogeneous population of small particles is:

$$\left.\frac{\partial N_s}{\partial t}\right|_{\text{aut}} = -\frac{1}{2}\frac{\rho_e}{q_e}\pi(2r_s)^2|\Delta w_s|\,E\,N_s^2 \qquad (23)$$

where the difference in fall velocities Δw_s is approximated using the dispersion $X=0.25$ of the fall velocity spectrum of small particles, as in Murakami (1990):

$$|\Delta w_s| = w_2(r_s)X \qquad (24)$$

For the fall velocity we use Eq. (11), which shows a linear radius dependence and applies to medium-sized

particles, i.e., larger than the particles in our small category. This introduces a small inconsistency but allows to linearize Eq. (23) as shown below. Using Eqs. (11) and (24) we get:

$$\left.\frac{\partial N_s}{\partial t}\right|_{\text{aut}} = -\frac{\rho_e}{q_e} c_{\text{aut}} N_s \tag{25}$$

where the parameter c_{aut} is given by:

$$c_{\text{aut}} = 3\sqrt{\frac{\rho_{e0}}{\rho_e}} q_s E \tag{26}$$

We assume that q_s is constant during the model time step in order to linearize Eq. (23). Eq. (25) can then be solved analytically for the characteristic time τ_{aut} that is needed for a small particle with the radius $\bar{r}_s$ to grow until it reaches the threshold radius $\bar{r}_{l0}$.

$$\tau_{\text{aut}} = -\frac{q_e}{\rho_e}\frac{1}{c_{\text{aut}}}\ln\left(\frac{N_{l0}}{N_s}\right) \tag{27}$$

Assuming that the growth rate for a particle with the radius $\bar{r}_s$ is representative of the whole distribution, this characteristic time is equal to the transfer time of all small particles. The total mass mixing ratio of the small mode is then transferred to the large one ($q_{l0}=q_s$) while the number concentration decreases from N_s to N_{l0}. The average particle mass of a single particle is given by the ratio of the mass mixing ratio and the particle number concentration. When the particle density ρ_s remains constant we have:

$$\frac{N_{l0}}{N_s} = \frac{q_{l0}\overline{M}_s}{q_s\overline{M}_{l0}} = \frac{\overline{M}_s}{\overline{M}_{l0}} = \frac{\bar{r}_s^3}{\bar{r}_{l0}^3} \tag{28}$$

where $\bar{M}_s$ and $\bar{M}_{l0}$ are the average masses for a single particle from the small class and for a particle with the threshold radius, respectively. We use this expression in Eq. (27) and obtain:

$$\tau_{\text{aut}} = -\frac{q_e}{\rho_e}\frac{1}{c_{\text{aut}}}\ln\left(\frac{\bar{r}_s}{\bar{r}_{l0}}\right)^3. \tag{29}$$

The decrease in the number concentration of small particles due to the autoconversion process is then given by:

$$\frac{\Delta N_s}{\Delta t} = -\frac{N_s}{\tau_{\text{aut}}}. \tag{30}$$

For the increase in the number concentration of the large class we get:

$$\left.\frac{\Delta N_l}{\Delta_t}\right|_{\text{aut}} = \frac{q_s}{\tau_{\text{aut}}\overline{M}_{l0}}. \tag{31}$$

For the change in mass mixing ratios we obtain:

$$-\left.\frac{\Delta q_s}{\Delta t}\right|_{\text{aut}} = \left.\frac{\Delta q_l}{\Delta t}\right|_{\text{aut}} = \frac{q_s}{\tau_{\text{aut}}}. \tag{32}$$

This concept has been applied to autoconversion of both the small warm and cold categories. The threshold radius $\bar{r}_{l0}$ is set to that of the radius of the large ash class in the presence of ash, or to 40 μm in the background atmosphere.

In an explosive eruption cloud, the large cold mode is the most prominent particle category, as we show in Paper II. The residence times of these particles are relatively long, because they are smaller than precipitating particles in meteorological clouds, and because of the great height of the volcanic umbrella cloud. Hence, in contrast to the usual concepts of cloud microphysical parameterization, we have to consider intramodal aggregation within the category of large cold particles. We employ the concept of autoconversion highlighted above. The decrease in number concentration is obtained from the discrete form of Eq. (25). The mass mixing ratio of newly aggregated particles (that do however not change category in this intra-modal process) is obtained by dividing this number by the original mass $\bar{M}_s$ of an individual particle in the large cold mode. The radius of average mass of the particles after intra-modal aggregation r_l is calculated from rearranging Eq. (29) where τ is given here by the model time step Δt:

$$\bar{r}_l = \bar{r}_s \exp\left(\frac{c_{\text{aut}}\Delta t}{3}\frac{\rho_e}{q_e}\right). \tag{33}$$

Using this radius we get the mass of an individual particle after aggregation $\bar{M}_l$ by which we divide the mass mixing ratio of newly aggregated particles and obtain the number concentration ΔN_l of newly aggregated particles during Δt. The net change of the number concentration in the large cold mode due to intra-modal aggregation is:

$$\left.\frac{\Delta N_p}{\Delta t}\right|_{\text{aut}} = \frac{\Delta N_l}{\Delta t} - \frac{\Delta N_s}{\Delta t} \tag{34}$$

The mass mixing ratio does not change, therefore this process leads to a shift of the radius of the large cold mode to greater values. In Paper II we show the effect of considering this process, and in a series of sensitivity studies we vary the collection coefficient in order to evaluate the influence on the ash aggregation rate.

4.7. Collection efficiency

The probability of successful aggregation during accretion or autoconversion of two particles (indices 1

and 2) is described by the collection efficiency E. It is equal to the product of collision efficiency E_{colli} and coalescence efficiency E_{coal}:

$$E = E_{\mathrm{colli}} \cdot E_{\mathrm{coal}}. \tag{35}$$

The collision efficiency E_{colli} is defined as the ratio of the numbers of theoretical collisions given by the geometrical cross-section $\pi (r_1+r_2)^2$ to actual collisions. The latter are influenced by inertial, aerodynamic and electrostatic forces. E is usually smaller than 1, but can exceed 1 for charged particles (Rogers and Yau, 1989; Pruppacher and Klett, 1997). The collision efficiency generally increases with increasing particle size because the forces of viscous deflection become less effective as the particle inertia increases. For colliding particles of equal size the relative velocities decrease thus prolonging the time for the viscous force to deflect the particles thus reducing E_{colli}. On the other hand, for larger particles (of order of 10 to 100 μm) with larger Reynolds numbers there is the possibility of 'wake capture' when the trailing particles fall into the wake of the leading particle. Wake capture tends to increase E_{colli}. Higher particle density and lower air density lead to more collisions, since the relative velocities increase, but also the collision efficiencies become larger (Khain, 1999). The collision efficiency is difficult to observe and shows a strong non-linear behavior. It is increased in turbulence flow (e.g., Falkovich et al., 2002) or electrostatic particle attraction (see Section 3). In the concept of this first study on aggregation in volcanic eruption columns, we assume for simplicity that the collision efficiency is independent of the effects of different particle sizes, shapes and turbulence. Please note that this only concerns the efficiency of collision as defined in the beginning of this section. The number of theoretical collisions is determined by the differential particle sizes and fall velocities in our study as explained in Section 4.6.1. For pure hydrometeors we use the collection efficiencies E_x given in the cloud microphysical literature (e.g., Wisner et al., 1972; Rogers and Yau, 1989; Pruppacher and Klett, 1997, among others). The coalescence efficiency for liquid water drops smaller than about 100 μm is usually assumed to be unity (Rogers and Yau, 1989) and we follow this approach for all collisions in which liquid water is involved. For ice particles the collection efficiency decreases with decreasing temperature (Lin et al., 1983):

$$E_x = \exp(0.05(T - T_0)). \tag{36}$$

We test the influence of the temperature on the aggregation of frozen particles in a sensitivity study in Paper II.

The collection efficiencies for the formation of mixed hydrometeor–ash particles E_{ax} in a volcanic cloud are unknown to date, but it probably depends on the hydrometeor availability at the particle's surface. In this study, we assume that hydrometeors act like an adhesive. As soon as particles are sufficiently covered by water or ice, they behave like pure hydrometeors. Volcanic ash is often non-spherical in shape and highly porous depending on magma type and on eruption style. Because of the limited knowledge about ash morphology, we do not attempt to explicitly calculate the amount of water or ice necessary to completely cover a particle. The collection efficiency for hydrometeor–ash aggregation E_{ax} is obtained by modifying E_x with simple functions, $f(\epsilon)$, reflecting the availability of hydrometeors at the particle surfaces:

$$E_{ax} = E_x \cdot f(\epsilon) \tag{37}$$

with $f(\epsilon) \leq 1$ to prevent the collection efficiency of mixed particles from exceeding that of pure hydrometeors. We suppose that the collection efficiency of two particles is determined by the particle with the higher mass ratio of hydrometeor and ash, q_x/q_{ax}. The relevant mass ratio of hydrometeor and ash is:

$$\epsilon = \max\left(\frac{q_{x1}}{q_{ax1}}, \frac{q_{x2}}{q_{ax2}}\right). \tag{38}$$

The aggregation of dry ash particles is neglected ($f(\epsilon)=0$) in the reference experiment. If the hydrometeor mass fraction in one of the colliding particles is larger than 50%, it is assumed that the layer of water (or ice) around the mixed particle is sufficiently thick to entirely cover the ash core in our reference experiment. From this threshold on ($\epsilon \geq 0.5$) the collection efficiencies for pure water hydrometeors are applied. For a solid, spherical ash particle of 50 μm in radius and a density of 1800 kg/m^3 such a hydrometeor layer around the ash core would have a diameter of $\Delta r = 20$ μm. For smaller amounts of hydrometeors, we assume in the reference experiment that the collection efficiency is linearly dependent on the hydrometeor mass fraction of the colliding particles and use $f_{\mathrm{REF}}(\epsilon)=\epsilon$. In a series of sensitivity studies discussed in Paper II we modify the collection efficiencies when we modify the functions f that reflect the availability of hydrometeors at the particle surfaces. In addition, particle rebounding and disintegration are neglected in this study, as no quantitative data on these processes exist.

Aggregation of small, dry ash particles is promoted by electrostatic forces, see Section 3. Within the concept of ATHAM it is however impossible at the moment to explicitly simulate such effects, because we do not calculate electric fields. In order to get a first appraisal of the potential importance of electrostatic effects, we perform a series of simplified experiments in which we allow for the autoconversion of dry ash particles in the small categories. Electrostatic forces are represented by using non-zero values for the collection efficiency in the absence of hydrometeors, where these forces are most relevant. Please note that our usual parameterization allows for aggregation only in the presence of water or ice. At locations where hydrometeors occur simultaneously with ash particles, we use the modified collection efficiencies for hydrometeors as highlighted above, and electrostatic effects are not considered. The numerical experiments on electrostatic aggregation are discussed in Paper II.

4.8. Melting and freezing

We presume that cloud ice melts instantaneously because it is small enough for heat to be transferred within one model time step, and forms cloud droplets if it is brought into areas where temperature is above freezing.

Melting of graupel is achieved by heat transfer through heat-conduction, water vapor diffusion and accretion of cloud or rain water (Mason, 1956) as described in Herzog et al. (1998). Melting graupel consists of an ice core surrounded by melt water. Depending on the fall velocity and the diameter of the ice spheres one can distinguish between different melting modes (Rasmussen et al., 1984). However, melting and shedding are not well quantified at the moment. It has been observed that ice particles shed their meltwater if they are larger than about 4.5 mm in radius (Rasmussen et al., 1984) due to hydro-dynamical imbalances. The fraction of melt water must be larger than a critical value of about 20% of the particle mass. The radius of drops resulting from meltwater shedding from hail or graupel is observed to be in the range of 0.25 to 1 mm with a 0.5 mm modal size (Rasmussen et al., 1984; Rasmussen and Heymsfield, 1987, among others). For simplicity, we assume in our experiment that liquid water from melting of graupel will be completely shed and transferred to rain. The number concentration of drops is determined by assuming that the shed size is $r_{\mathrm{shed}}=0.5$ mm, but not larger than the graupel radius, $\bar{r}_h$. The number concentration of graupel does not change during melting, except for total melting of pure graupel that is unpolluted with volcanic ash.

For the parameterization of freezing of (supercooled) water, we follow the stochastic hypothesis of Bigg (1953) and Barklie (1959) as described in Herzog et al. (1998). Freezing does not change the total number concentration of the particles involved, but the particles change from a liquid to a frozen category. Water contained in the hydrometeor–ash aggregates is assumed to melt or freeze like pure water hydrometeors.

Corresponding fractions of volcanic ash in mixed hydrometeor–ash aggregates are transferred to the respective melted or frozen categories, as given by Eqs. (14) and (15).

5. Discussion and conclusions

The microphysics of frozen and liquid hydrometeors and of ash particles is described in this paper. We introduce the processes in explosive volcanic eruption columns in the atmosphere after the decompression phase that lead to particle aggregation, and we present the parameterizations employed in the ATHAM model to simulate these processes. In the following we summarize our parameterizations and discuss their shortcomings.

Volcanic particles are assumed to be active as nuclei for liquid and ice clouds, because ash is often covered with hygroscopic salts, and because of the high supersaturation caused by the extreme vertical velocity within the eruption column. More detailed information on the nucleation capacities of volcanic particles both for liquid water and ice would however be desirable in order to refine our parameterization. We do not consider the co-existence of dry ash, pure hydrometeors and mixed aggregates at the same location at a given model time step. Instead particles are always contained in mixed hydrometeor–ash aggregates. The advantage of this simplification is an enormous reduction of the number of tracers and equations that we have to consider for transport and microphysical processes. In reality though, it is possible that not all ash particles are activated, for several reasons: firstly because of the extremely high concentrations within the eruption column; secondly because of the limited availability of condensed hydrometeors when compared to the amount of volcanic ash during typical Plinian eruptions (see Paper II), and thirdly because some particles are fairly large. Preferential activation would result in preferential growth of fewer hydrometeor-coated particles, and less aggregates, which are however larger, would form. Modifications of the aggregation process allowing for

the co-existence of inactive ash particles and pure hydrometeors with mixed aggregates are however outside the scope of our model concept at the moment.

We consider two size classes of particles, each in a liquid and a frozen category. The particles in these four categories can have any fraction of hydrometeors and volcanic ash. Mixed hydrometeor–ash aggregates take part in all the microphysical processes, and corresponding fractions of the two components are transferred among the particle categories. All effects of latent heat release from any phase transfer of water on the plume dynamics are considered. The particle size distributions are represented by generalized gamma functions with prescribed skewness. A more complete representation of the microphysics would describe the size distribution with a higher number of modes or moments (thus considering changes in the skewness of the size distribution), or with a spectral approach where the microphysics and transport processes are explicitly calculated for many small size intervals. However, the application of these methods to simulations of eruption columns results in much higher requirements of computing time and memory. We currently implement the spectral microphysical approach of Khain and Sednev (1995, 1996) into a parallelized version of the ATHAM model (Herzog et al., 2000, 2003).

Gravitational capture is the dominant process leading to particle collision, because volcanic particles are of contrasting size. The particle fall velocity depends on the particle size and density, and on the density of the ambient air. The density of aggregates is approximated by a linear combination of water and ash, potential air bubbles are neglected. Particles are treated like rigid spheres, because we do only have limited information about the particle shapes. The shape effect on the fall velocity is only considered by applying a drag coefficient. This might cause a small overestimation of the fall speed. Lane et al. (1993) performed laboratory experiments showing that the fall velocities of aggregates and single particles can be modeled in the same way using the reduced aggregate density and the size corresponding to the enclosing sphere. The implementation of results from the extensive study of Riley et al. (2003) on the relationship between size, shape and terminal fall velocity of volcanic particles will be explored in future ATHAM experiments.

Aggregation is caused by the interaction between volcanic ash and hydrometeors in this study. The collection efficiency for aggregate formation is assumed to depend on the fraction of water or ice available at the particle surfaces. The amount of hydrometeors can be influenced by the presence of dissolved species that modify the thermodynamic properties of hydrometeors (salinity effects). The principal importance of salinity effects is discussed in Paper II. The amount of hydrometeors depends also on the porosity and permeability of ash, since water can diffuse into the inner core of permeable particles. This reduces the amount of water or ice available at the surface until the particle is 'saturated'. We make simple assumptions on how the collection efficiencies depend on the ash–hydrometeor ratio and investigate the sensitivity of ash aggregation to these assumptions in numerical experiments in Paper II. Our experiments provide indirect insights into the sensitivity of the aggregation process on the ash porosity. Furthermore, ATHAM does not capture electrostatic aggregation within the conduit or close to the vent, because simulations start after adjustment to ambient pressure values (see Paper II for a more detailed description of the ATHAM model). The importance of electrostatic effects on aggregation during transport within the eruption column is investigated in Paper II. These first numerical experiments on electrostatic volcanic ash aggregation are based on simplifying parameterizations. A more comprehensive study of such effects requires a major extension of the ATHAM model in order to simulate electric fields and is outside the scope of this study.

As no quantitative data on the stability of aggregates are available, disintegration has been neglected so far. We also neglect the process of ice multiplication (i.e., the increase in number of ice crystals by fragmentation into small, pure ice crystals, see Pruppacher and Klett (1997)). Ice multiplication is most important between -3 and -8 °C. Due to the very fast plume ascent, the residence time in this temperature zone is short, and ice multiplication can be assumed to be insignificant in explosive volcanic eruption columns. In addition, no studies exist about ice multiplication of heavily polluted ash–hydrometeor aggregates.

The parameterizations for the particle microphysics used in this study have been developed for meteorological clouds under normal atmospheric conditions that are very different from the extreme conditions within a volcanic eruption column. For example the collection efficiency might be modified by the highly turbulent conditions or electrostatic effects prevailing in eruption columns. Information on the properties of volcanic ash in the eruption column is currently very limited. Future studies in the field as well as in the laboratory are necessary to evaluate our approaches relating to the aggregation process of volcanic particles. Our treatment of mixed aggregates as pure hydrome-

teors as well as neglecting aggregate disintegration might cause overestimation of particle growth. At the same time, neglecting electrostatics and salinity effects might cause an underestimation. However, despite these potential reservations, the numerical experiments with the ATHAM model presented in Paper II allow us for the first time to investigate the individual parameters that control ash aggregation within Plinian eruption columns. The implementation of results gained from our numerical experiments can help to identify important parameters which should be scrutinized, and help to design experimental setups.

Acknowledgments

C. Textor, H.-F. Graf and M. Herzog thank the Volkswagen Foundation for supporting the development of the ATHAM model. C. Textor thanks M. Schulz and the Laboratoire des Sciences du Climat et de l'Environnement for the opportunity to complete this study. G.G.J. Ernst thanks the Max-Planck-Institut für Meteorologie for welcoming him in the Hamburg group and for generous financial support. He also thanks the Fondation Belge de la Vocation (Golden Clover Award), the Nuffield Foundation (NAL award), and the Belgian NSF (FWO-Vlaanderen) for current support at U. Ghent. We would also like to thank the two anonymous reviewers, especially for indicating the importance of electrostatic and hygroscopic effects.

References

Armienti, P., Macedonio, G., Pareschi, M.T., 1988. A numerical model for simulation of tephra transport and deposition: applications to May 18, 1980, Mount St. Helens eruption. Journal of Geophysical Research 93 (B6), 6463–6476.

Barberi, F., Macedonio, G., Pareschi, M., Santacroce, R., 1990. Mapping the tephra fallout risk: an example from Vesuvius, Italy. Nature 344, 142–144.

Barklie, R.H.D., 1959. Nucleation measurements on rain and melted hail. Sci. Rep. MW-30, Stormy Weather Research Group, McGill University.

Beheng, K.D., 1994. A parameterization of warm cloud microphysical conversion processes. Atmospheric Research 33, 193–206.

Beheng, K.D., Doms, G., 1990. A general formulation of collection rates of cloud and raindrops using the kinetic equation and comparison with parameterizations. Beiträge zur Physik der Atmosphäre 59 (1), 66–84.

Berry, E.X., Reinhardt, R.L., 1974. An analysis of cloud drop growth by collection: Part IV: A new parameterization. Journal of the Atmospheric Sciences 31 (46), 2127–2135.

Bigg, E.K., 1953. The supercooling of water. Proceedings of the Physical Society B66, 688–694.

Bonadonna, C., Phillips, J., 2003. Sedimentation from strong volcanic plumes. Journal of Geophysical Research 108 (B7) Art. No. 2340.

Bonadonna, C., Ernst, G.G.J., Sparks, R.S.J., 1998. Thickness variations and volume estimates of tephra fall deposits: the importance of particle Reynolds number. Journal of Volcanology and Geothermal Research 81, 173–187.

Bonadonna, C., Calder, E., Choux, C., Jackson, P., Lejeune, A., Loughlin, S., Mayberry, G., Norton, G., Rose, W., Ryan, G., Sparks, R.S.J., Young, S., 2002a. Tephra fallout in the eruption of the Soufrière Hills Volcano, Montserrat. In: Druitt, T., Kokelaar, P. (Eds.), The Eruption of Soufrière Hills Volcano, Montserrat, 1995–1999. Memoir Vol. 21. Geological Society of London, pp. 483–516.

Bonadonna, C., Macedonio, G., Sparks, R.S.J., 2002b. Numerical modelling of tephra fallout associated with dome collapses and vulcanian explosions—application to hazard assessment on Montserrat. In: Druitt, T., Kokelaar, P. (Eds.), The Eruption of Soufriére Hills Volcano, Montserrat, 1995–1999. Memoir Vol. 21. Geological Society of London, pp. 517–537.

Bursik, M.I., 1998. Tephra dispersal. In: Gilbert, J.S., Sparks, R.S.J. (Eds.), The physics of explosive volcanic eruptions, Geological Society Vol. 145. Special Publications, London, pp. 115–144.

Bursik, M.I., Sparks, R.S.J., Gilbert, J.S., Carey, S.N., 1992. Sedimentation of tephra by volcanic plumes I: Theory and its comparison with a study of the Fogo A Plinian deposit Sao Miguel (Azores). Bulletin of Volcanology 54, 329–344.

Byers, H.R., 1965. Elements of cloud physics. The University of Chicago Press.

Carey, S., Sigurdsson, H., 1982. Influence of particle aggregation on deposition of distal tephra from the May 18, 1980, eruption of Mount St. Helens volcano. Journal of Geophysical Research 87 (B8), 7061–7072.

Carey, S., Sparks, R.S.J., 1986. Quantitative models of the fallout and dispersal of tephra from volcanic eruption columns. Bulletin of Volcanology 48, 109–125.

Clarke, A.B., Voight, B., Neri, A., Macedonio, G., 2002. Transient dynamics of vulcanian explosions and column collapse. Nature 415, 897–901.

Dobran, F., Neri, A., 1993. Numerical simulation of collapsing volcanic columns. Journal of Geophysical Research 98, 4231–4259.

Durant, A.D., Ernst, G.G.J., submitted for publication. Formation of accretionary lapilli as volcanogenic hailstones. Bulletin of Volcanology.

Durant, A.J., Swanson, D.A., Rose, W.I., 2002. Accretionary lapilli beds in the Keanakako'i ash: Footprint bearing beds not 1790 in age. Eos Transactions of AGU 83 (47) Abstract V12B-1433.

Ernst, G.G.J., Davis, J.P., Sparks, R.S.J., 1994. Bifurcation of volcanic plumes in a crosswind. Bulletin of Volcanology 56 (3), 159–169.

Ernst, G.G.J., Carey, S.N., Bursik, M.I., Sparks, R.S.J., 1996. Sedimentation from turbulent jets and plumes. Journal of Geophysical Research 101, 5575–5589.

Falkovich, G., Fouxon, A., Stepanov, M., 2002. Acceleration of rain initiation by cloud turbulence. Nature 419, 151–154.

Flatau, P.J., Tripoli, G.J., Verlinde, F., Cotton, W.R., 1989. The CSU-RAMS cloud microphysical module: General theory and code documentation. Atmospheric Science Paper 451 88 pp.

Fletcher, N.H., 1962. The Physics of Rainclouds. Cambridge University Press.

Gilbert, J.S., Lane, S.J., 1994. The origin of accretionary lapilli. Bulletin of Volcanology 56, 398–411.

Gilbert, J.S., Lane, S.J., Sparks, R.S.J., Koyaguchi, T., 1991. Charge measurements on particle fallout from a volcanic plume. Nature 349, 598–600.

Glaze, L., Self, S., 1990. Ashfall dispersal for the 16 September 1986 eruption of Lascar, Chile, calculated by a turbulent diffusion model. Geophysical Research Letters 18, 1237–1240.

Glaze, L.S., Baloga, S.M., Wilson, L., 1997. Transport of atmospheric water vapor by volcanic eruption columns. Journal of Geophysical Research 102 (D5), 6099–6108.

Graf, H.-F., Herzog, M., Oberhuber, J.M., Textor, C., 1999. The effect of environmental conditions on volcanic plume rise. Journal of Geophysical Research 104, 24309–24320.

Gunn, R., Kinzer, G.D., 1949. The terminal velocity of fall for water drops in stagnant air. Journal of Meteorology 6, 243–248.

Guo, S., Bluth, G.J.S., Rose, W.I., Watson, I.M., Prata, A.J., 2004a. Reevaluation of SO_2 release of the climactic June 15, 1991 Pinatubo eruption using TOMS and TOVS satellite data. Geochemistry, Geophysics, Geosystems 5. doi:10.1029/2003GC000654 (4, Q04001).

Guo, S., Rose, W.I., Bluth, G.J.S., Watson, I.M., 2004b. Particles in the great Pinatubo volcanic cloud of June 1991: the role of ice. Geochemistry, Geophysics, Geosystems 5. doi:10.1029/2003GC000655 (5, Q05003).

Herzog, M., Graf, H.-F., Textor, C., Oberhuber, J.M., 1998. The effect of phase changes of water on the development of volcanic plumes. Journal of Volcanology and Geothermal Research 87, 55–74.

Herzog, M., Textor, C., Antonelli, M., 2000. Modelling volcanic eruption plumes. HPC News 13.

Herzog, M., Oberhuber, J.M., Graf, H., 2003. A prognostic turbulence scheme for the non-hydrostatic plume model ATHAM. Journal of the Atmospheric Sciences 60, 2783–2796.

Hobbs, P.V., Tuell, J.P., Hegg, D.A., Radke, L.F., Eltgroth, M.W., 1982. Particles and gases from the 1980–1981 volcanic eruptions of Mount St. Helens. Journal of Geophysical Research 87, 11062–11086.

Isono, K., Komabayasi, M., Ono, A., 1959. Volcanoes as a source of atmospheric ice nuclei. Nature 183 (4657), 317–318.

James, M.R., Gilbert, J.S., Lane, S.J., 2000. Volcanic plume electrification: Experimental investigation of a fracture-charging mechanism. Journal of Geophysical Research 105 (B7), 16641–16649.

James, M.R., Gilbert, J.S., Lane, S.J., 2002. Experimental investigation of volcanic particle aggregation in the absence of a liquid phase. Journal of Geophysical Research 107 (B9), doi:10.1029/2001JB000950.

James, M.R., Lane, S.J., Gilbert, J.S., 2003. Density, construction, and drag coefficient of electrostatic volcanic ash aggregates. Journal of Geophysical Research 108 (B9). doi:10.1029/2002JB002011.

Kaminski, E., Jaupart, C., 1998. The size distribution of pyroclasts and the fragmentation sequence in explosive volcanic eruptions. Journal of Geophysical Research 103, 29759–29779.

Khain, A.P., 1999. personal communication.

Khain, A.P., Sednev, I., 1995. Simulation of hydrometeor size spectra evolution by water–water, ice–water and ice–ice interactions. Atmospheric Research 36, 107–138.

Khain, A.P., Sednev, I., 1996. Simulation of precipitation formation in the eastern Mediterranean coastal zone using a spectral microphysics cloud ensemble model. Atmospheric Research 43, 77–110.

Koyaguchi, T., Ohno, M., 2001. Reconstruction of eruption column dynamics on the basis of grain size of tephra fall deposits 1. Methods. Journal of Geophysical Research 106 (B4), 6499–6512.

Krotkov, N., Flittner, D., Krueger, A., 1999. Effect of particle nonsphericity on satellite monitoring of drifting volcanic ash clouds. Journal of Quantitative Spectroscopy and Radiative Transfer 63 (2–6), 613–630.

Lacasse, C., Karlsdóttir, S., Larsen, G., Soosalu, H., Rose, W.I., Ernst, G.G.J., 2004. Weather radar observations of the Hekla 2000 eruption cloud, Iceland. BV 66, 457–473.

Lane, S.J., Gilbert, J.S., 1992. Electric potential gradient changes during explosive activity at Sakurajima volcano, Japan. Bulletin of Volcanology 54 (7), 590–594.

Lane, S.J., Gilbert, J.S., Hilton, M., 1993. The aerodynamic behaviour of volcanic aggregates. Bulletin of Volcanology 55, 481–488.

Lin, Y., Farley, R.D., Orville, H.D., 1983. Bulk parameterization of the snow field in a cloud model. Journal of Climate and Applied Meteorology 22, 1065–1092.

Lüpkes, C., 1991. Untersuchungen zur Parametrisierung von Koagulationsprozessen von niederschlagsbildenden Tropfen. Verlag Dr. Kovac, Hamburg.

Mackinnon, I.D.R., Gooding, J.L., McKay, D.S., Clanton, U.S., 1984. The El Chichón stratospheric cloud: solid particulates and settling rates. Journal of Volcanology and Geothermal Research 23, 125–1246.

Mason, B.J., 1956. On the melting of hailstones. Quarterly Journal of the Royal Meteorological Society 82, 209–216.

Mayberry, G.C., Rose, W.I., Bluth, G.J.S., 2003. Dynamics of the volcanic and meteorological clouds produced by the December 26, 1997 eruption of Soufrière Hills Volcano, Montserrat, W.I. In: Druitt, T., Kokelaar, P. (Eds.), The Eruption of Soufrière Hills Volcano, Montserrat, 1995–1999. Memoir Vol. 21. Geological Society of London, pp. 539–555.

Meyers, M.P., Walko, R.L., Harrington, J.Y., Cotton, W.R., 1997. New RAMS cloud microphysics parameterization. Part II: The two moment scheme. Atmospheric Research 45, 3–39.

Molenkamp, C.R., Bradley, M.M., 1990. Parameterization of aerosol scavenging in a convective cloud model. Preprints, American Meteorological Society 1990 Conference on Cloud Physics, San Francisco, CA, July 23–27, pp. 403–407.

Murakami, M., 1990. Numerical modeling of dynamical and microphysical evolution of an isolated convective cloud—The 19 July 1981 CCOPE Cloud. Journal of Meteorological Society of Japan 68 (2).

Neri, A., Macedonio, G., 1996. Numerical simulation of collapsing volcanic columns with particles of two sizes. Journal of Geophysical Research 101, 8153–8174.

Neri, A., Ongaro, T.E., Macedonio, G., Gidaspow, D., 2002. Multiparticle simulation of collapsing volcanic columns and pyroclastic flow. Journal of Geophysical Research 108 (B4), doi:10.1029/2001JB000508.

Oberhuber, J.M., Herzog, M., Graf, H.-F., Schwanke, K., 1998. Volcanic plume simulation on large scales. Journal of Volcanology and Geothermal Research 87, 29–53.

Pruppacher, H.R., Klett, J.D., 1997. Microphysics of Clouds and Precipitation. (2nd Edition)Kluwer Academic Publishers.

Rasmussen, R.M., Heymsfield, A.J., 1987. Melting and shedding of graupel and hail. Part III: Investigation of the role of shed drops as hail embryos in the 1 August CCOPE severe storm. Journal of the Atmospheric Sciences 44 (19), 2783–2803.

Rasmussen, R.M., Levizzani, V., Pruppacher, H.R., 1984. A wind tunnel and theoretical study on the melting behaviour of atmospheric ice particles: experiment and theory for spherical ice particles of radius <500 μm. Journal of the Atmospheric Sciences 41 (3), 381–388.

Riedel, C., Ernst, G.G.J., Riley, M., 2003. Controls on the growth and geometry of pyroclastic constructs. Journal of Geophysical Research 127 (1–2), 121–152.

Riley, C.M., Rose, W.I., Bluth, G.J.S., 2003. Quantitative shape measurements of distal volcanic ash. Journal of Geophysical Research 108 (B10) Art. No. 2504.

Robock, A., 2000. Volcanic eruptions and climate. Reviews of Geophysics 38, 191–219.

Rogers, R.R., Yau, M.K., 1989. A Short Course on Cloud Physics. (3rd Edition)Pergamon Press, Oxford.

Rose, W.I., 1977. Scavenging of volcanic aerosol by ash: atmospheric and volcanological implications. Geology 5, 621–624.

Rose, W.I., Bluth, G.J.S., Ernst, G.G.J., 2000. Integrating retrievals of volcanic cloud characteristics from satellite remote sensors: a summary. Philosophical Transactions of the Royal Society of London Series A—Mathematical Physical and Engineering Sciences 358, 1538–1606.

Rose, W.I., Bluth, G.J.S., Schneider, D.J., Ernst, G.G.J., Riley, C.M., Henderson, L.J., McGimsey, R.G., 2001. Observations of volcanic clouds in their first few days of atmospheric residence: The 1992 eruptions of Crater Peak, Mount Spurr volcano, Alaska. Journal of Geology 6, 677–694.

Rose, W.I., Chuan, R.L., Woods, D.C., 1982. Small particles in the plumes of Mount St. Helens. Journal of Geophysical Research 87 (C7), 4956–4962.

Rose, W.I., Delene, D., Schneider, D., Bluth, G., Krueger, A., Sprod, I., McKee, C., Davies, H., Ernst, G.G.J., 1995. Ice in the 1994 Rabaul eruption cloud: implications for volcano hazard and atmospheric effects. Nature 375, 477–479.

Rose, W.I., Gu, Y., Watson, I., Yu, T., Bluth, G., Prata, A., Krueger, A., Krotokov, N., Carn, S., Fromm, M., Hunton, D., Viggiano, A., Miller, T., Balletin, J., Ernst, G.G.J., Reeves, J., Wilson, C., Anderson, B., 2003. The February–March 2000 eruption of Hekla, Iceland, from a satellite perspective. In: Robock, A., Oppenheimer, C. (Eds.), Volcanism and the Earth Atmosphere, AGU Geophysical Monograph Vol. 139, pp. 107–132.

Schneider, D.J., Rose, W.I., Coke, L.R., Bluth, G.J.S., 1999. Early evolution of a stratospheric volcanic eruption cloud as observed with TOMS and AVHRR. Journal of Geophysical Research 104 (D4), 4037–4050.

Schnell, R.C., Delany, A.C., 1976. Airborne ice nuclei near an active volcano. Nature 264 (5586), 535–536.

Schumacher, R., 1994. A reappraisal of Mount St. Helens ash clusters—depositional model from experimental observation. Journal of Volcanology and Geothermal Research 59, 253–260.

Schumacher, R., Schmincke, H.-U., 1991. Internal structure and occurrence of accretionary lapilli—a case study at Laacher See Volcano. Bulletin of Volcanology 53, 612–634.

Schumacher, R., Schmincke, H.-U., 1995. Models for the origin of accretionary lapilli. Bulletin of Volcanology 56, 626–639.

Seinfeld, J.H., Pandis, S.N., 1997. Atmospheric chemistry and physics Ch. 7. Wiley Interscience publication, p. 420.

Self, S., Sparks, R.S.J., 1978. Characteristics of widespread pyroclastic deposits formed by the interaction of silicic magma and water. Bulletin of Volcanology 41, 196–212.

Shaw, R.A., Durant, A.J., Mi, Y., 2005. Heterogeneous Surface crystallization observed in undercooled water. Journal of Physical Chemistry B 109, 9865–9868.

Smith, B.D., Zielinski, R.A., Rose, W.I., Huebert, B.J., 1982. Water-soluble material on aerosols collected within volcanic eruption clouds. Journal of Geophysical Research 87 (C7), 4963–4972.

Sorem, R.K., 1982. Volcanic ash clusters: Tephra rafts and scavengers. Journal of Volcanology and Geothermal Research 13, 63–71.

Sparks, R.S.J., Bursik, M.I., Ablay, G., Thomas, R.E., Carey, S.N., 1992. Sedimentation of tephra by volcanic plumes. Part 2: controls on thickness and grain-size variations of tephra fall deposits. Bulletin of Volcanology 54, 685–695.

Sparks, R.S.J., Bursik, M.I., Carey, S.N., Gilbert, J.S., Glaze, L., Sigurdsson, H., Woods, A.W., 1997. Volcanic Plumes. Wiley and Sons, New York.

Sparks, R.S.J., Carey, S.N., Sigurdsson, H., 1991. Sedimentation from gravity currents generated by turbulent plumes. Sedimentology 38, 839–856.

Symonds, R.B., Rose, W.I., Reed, M.H., 1988. Contribution of Cl- and F-bearing gases to the atmosphere by volcanoes. Nature 334, 415–418.

Textor, C., 1999. Numerical simulation of scavenging processes in explosive volcanic eruption clouds. PhD thesis, University of Hamburg.

Textor, C., Ernst, G.G.J., 2004. Comment on "Particle aggregation in volcanic eruption columns" by Graham Veitch and Andrew W. Woods, Journal of Geophysical Research—Solid Earth, 106 (B11), 26.425–26.441, 2001. Journal of Geophysical Research 109 (B05202), doi:10.1029/2002JB002291.

Textor, C., Graf, H., Longo, A., Neri, A., Ongaro, T., Papale, P., Timmreck, C., Ernst, G.G.J., in press. Numerical simulation of explosive volcanic eruptions from the conduit flow to global atmospheric scales. Annales of Geophysics.

Textor, C., Graf, H.-F., Herzog, M., Oberhuber, J.M., 2003. Injection of gases into the stratosphere by explosive volcanic eruptions. Journal of Geophysical Research 108 (D19). doi:10.1029/2002JD002987.

Textor, C., Graf, H.-F., Timmreck, C., Robock, A., 2004. Emissions from volcanoes. In: Granier, C., Reeves, C., Artaxo, P. (Eds.), Emissions of Chemical Compounds and Aerosols in the Atmosphere, Advances in Global Change Research Vol. 18. Kluwer, Dordrecht, pp. 269–303.

Textor, C., Sachs, P.M., Hansteen, T.H., 2003. The 12,900 yr BP Laacher See eruption: estimation of volatile yields and simulation of their fate in the plume. In: Oppenheimer, C., Pyle, D., Barclay, J. (Eds.), Volcanic Degassing, Geological Society Vol. 213. Special Publications, London, pp. 307–328.

Textor, C., Graf, H.-F., Herzog, M., Oberhuber, J.M., Rose, W.I., Ernst, G.G.J., 2005. Volcanic particle aggregation in explosive eruption columns. Part II: numerical experiments. Journal of Volcanology and Geothermal Research 150, 378–394 (this issue). doi:10.1016/j.jvolgeores.2005.09.008.

Twomey, S., Wojciechowski, T., 1969. Observations of the geographical variation of cloud nuclei. Journal of the Atmospheric Sciences 26, 684–688.

Valentine, G.A., Wohletz, K.H., 1989. Numerical models of Plinian columns and pyroclastic flows. Journal of Geophysical Research 94, 1867–1887.

Varekamp, J.C., Thomas, E., Germani, M., Buseck, P.R., 1986. Particle geochemistry of volcanic plumes of Etna and Mount St. Helens. Journal of Geophysical Research 91 (B12), 12233–12248.

Veitch, G., Woods, A.W., 2000. Particle recycling and oscillations of volcanic eruption columns. Journal of Geophysical Research 105 (B2), 2829–2842.

Veitch, G., Woods, A.W., 2001. Particle aggregation in volcanic eruption columns. Journal of Geophysical Research 106 (B1), 26425–26441.

Veitch, G., Woods, A.W., 2002. Particle recycling in volcanic plumes. Bulletin of Volcanology 64 (1), 31–39.

Veitch, G., Woods, A.W., 2004. Reply to comment by C. Textor and G.G.J. Ernst on particle aggregation in volcanic eruption columns. Journal of Geophysical Research 109 (B5) Art. No. B05203.

Verlinde, F., Flatau, P.J., Cotton, W.R., 1990. Analytical solutions to the collection growth equation: Comparison with approximate methods and application to cloud microphysics parameterization schemes. Journal of the Atmospheric Sciences 47, 2871–2880.

Walker, G.P.L., Wilson, L., Bowell, E.L.G., 1971. Explosive volcanic eruptions—I. The rate of fall of pyroclasts. Geophysical Journal of the Royal Astronomical Society 22, 377–383.

Walko, R.L., Cotton, W.R., Meyers, M.P., Harrington, J.Y., 1995. New RAMS cloud microphysics parameterization. Part I: The single moment scheme. Atmospheric Research 38, 29–62.

Wen, S., Rose, W.I., 1994. Retrieval of sizes and total masses of particles in volcanic clouds using AVHRR bands 4 and 5. Journal of Geophysical Research 99 (D3), 5421–5431.

Wiesner, M.G., Wang, Y., Zheng, L., 1995. Fallout of volcanic ash to the deep South China Sea induced by the 1991 eruption of Mount Pinatubo (Philippines). Geology 23 (10), 885–888.

Willis, P., 1984. Functional fits to some observed drop size distributions and parameterization of rain. Journal of the Atmospheric Sciences 41 (9), 1648–1661.

Wilson, L., 1976. Explosive volcanic eruptions—III. Plinian eruption columns. Geophysical Journal of the Royal Astronomical Society 45, 543–556.

Wilson, L., Huang, T.C., 1979. The influence of shape on the atmospheric settling velocity of volcanic ash particles. Earth and Planetary Science Letters 44, 311–324.

Wisner, C., Orville, H.D., Myres, C., 1972. A numerical model of a hail-bearing cloud. Journal of the Atmospheric Sciences 29, 1160–1181.

Wohletz, K.H., McGetchin, T.R., Sanford, M.T., Jones, E.M., 1984. Hydrodynamic aspects of caldera-forming eruptions: numerical models. Journal of Geophysical Research 89, 8269–8285.

Woods, A.W., 1988. The fluid dynamics and thermodynamics of eruption columns. Bulletin of Volcanology 50, 169–193.

Woods, A.W., 1993. Moist convection and the injection of volcanic ash into the atmosphere. Journal of Geophysical Research 98, 17627–17636.

Woods, A.W., Bower, S., 1995. The decompression of volcanic jets in craters. Earth and Planetary Science Letters 131, 189–205.

Woods, A.W., Bursik, M.I., 1991. Particle fallout, thermal disequilibrium and volcanic plumes. Bulletin of Volcanology 53, 559–570.